Supplementary material

$[(H_2O)(terpy)Mn(\mu\text{-}O)_2Mn(terpy)(OH_2)](NO_3)_3$ (terpy = 2,2':6,2''-terpyridine) and its relevance to the oxygen-evolving complex of photosystem II examined through pH dependent cyclic voltametry.

Clyde W. Cady[‡], Katherine E. Shinopoulos, Robert H. Crabtree* and Gary W. Brudvig*

Department of Chemistry, Yale University, P. O. Box 208107, New Haven, CT 06520-8107

*To Whom Correspondence Should be Addressed.

E-mail Addresses: robert.crabtree@yale.edu; gary.brudvig@yale.edu.

S1.0 Basal plane graphite electrode

The basal plane carbon-working electrode (Figure S1) was made by gluing a 1 cm square block of basal plane carbon to a brass rod sheathed in Teflon. The carbon to brass bond was made using two part silver conductive adhesive (purchased from VWR). The carbon block was then further affixed by encasing it in an epoxy resin (resin consisted of Araldite 506 epoxy resin, dodecenylsuccinic anhydride 90%, and 2,4,6-tris (dimethylaminomethyl)phenol, all purchased from Aldrich and used as received).

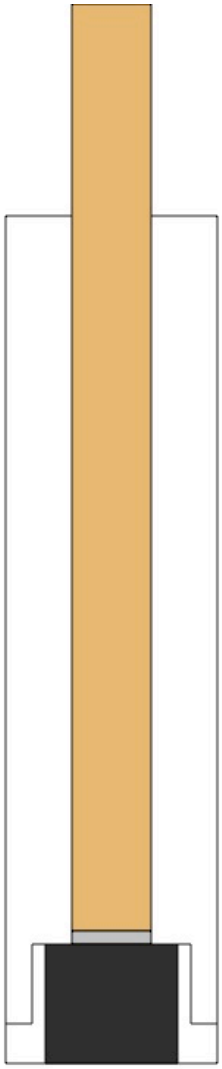

Figure S1 Cross-sectional view of a carbon electrode. The yellow color denotes brass, black represents the carbon block used for the surface of the working electrode, grey denotes the silver conducting epoxy used to create the bond between brass and carbon and white denotes Teflon and epoxy.

S2.0 measuring the P_a^1 peak in unbuffered solution

We measured the pH dependence of **1** without buffer up to a pH of approximately 5.5 at which point **1** decomposed. Graphing the unbuffered data revealed an unforeseen difficulty. The unbuffered pH dependent data does not fit a straight line (Figure 3.9). Looking at the original CV data it is apparent that the oxidation peak becomes increasingly broad in the unbuffered system. The original purpose of the terpyridine buffer was to increase the stability of **1** so we started to investigate if this broadness was due to decomposition of **1**.

As discussed in Chapter 2 of this thesis, disproportionation of the dimeric **1** into Mn(II) and Mn(IV) dimers is a constant concern with our oxo bridged systems.[9,27-29] The first control experiment that we ran, knowing of this tendency to disproportionate, was the CV of aqueous Mn(II). It became immediately apparent that free Mn(II) in water is oxidized at almost the same potential as **1** (Figure S2). The pH dependence of the aqueous Mn(II) oxidation matches nicely with the unbuffered data for **1** at higher pH (Figure S2). The control experiments with Mn(II) appear to show that $Mn(II)(H_2O)_6$ is the problem in an unbuffered solution of **1**. Closer examination of the earlier terpy buffered data showed that the buffer did not prevent the formation of the Mn(II) but was instead complexing the aqueous ions forming $(terpy)Mn(II)(H_2O)_3$. The Mn(II/III) couple of $(Terpy)Mn(II)(H_2O)_3$ has a much lower reduction potential than the hexaaquo species, which removes the Mn(II) impurity signal from our area of interest.

Once the impurity was identified, the challenge became isolating the signal for **1**. A standard method for deconvoluting spectroscopic peaks uses a computer program to fit the raw data to multiple ideal line shapes. In electrochemistry, this task is complicated by two factors. Firstly, aqueous electrochemistry peaks do not fit common line shapes such as Gaussians; they

are instead based on diffusion rates which are often much more difficult to model. Secondly, a standard CV in solution does not have a flat baseline.

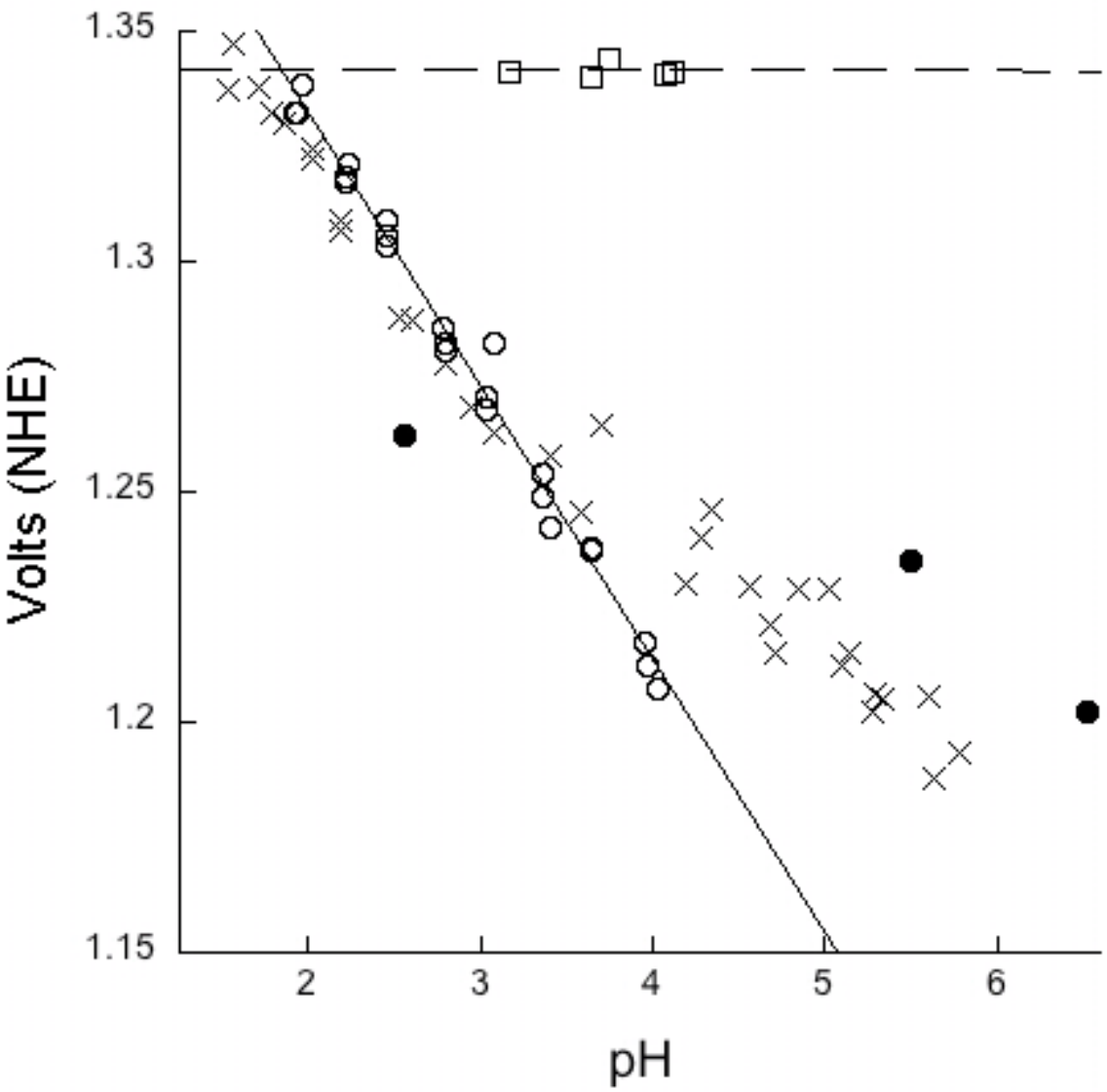

Figure S2 The potential for the oxidation of **1** vs. pH ploted showing buffered **1** (open circles) and **2** (squares) along side unbuffered **1** (X) and $Mn(II)(H_2O)_6$ (filled circles). The solid line represents a 59 mV/pH slope. All CVs taken at a basal plane graphite electrode in H_2O + 0.1 M KNO_3 scanned at 40 mV/s.

The solution to the first problem lay in finding an ideal oxidation peak for **1**. Isolating the oxidation peak for **1** at low pH or in buffer resulted in an ideal peak shape for **1** free of Mn(II) impurity. This peak could then be scaled and subtracted from the crude data. The second problem of flattening the baseline was solved by using the program "Utilities for Data Analysis 010716" by Dirk Herring to run a cubic splines baseline, which artificially flattens the baseline allowing for much easier data fitting. Figure S3A shows the raw data for a scan contaminated with aqueous Mn(II), while Figure S3B shows the data after it is baseline-corrected and fit. After data work-up, the result is shown in Figure 4A where it can now be seen that **1** in unbuffered solution does follow a 59 mV/pH slope up to biologically relevant values of pH.

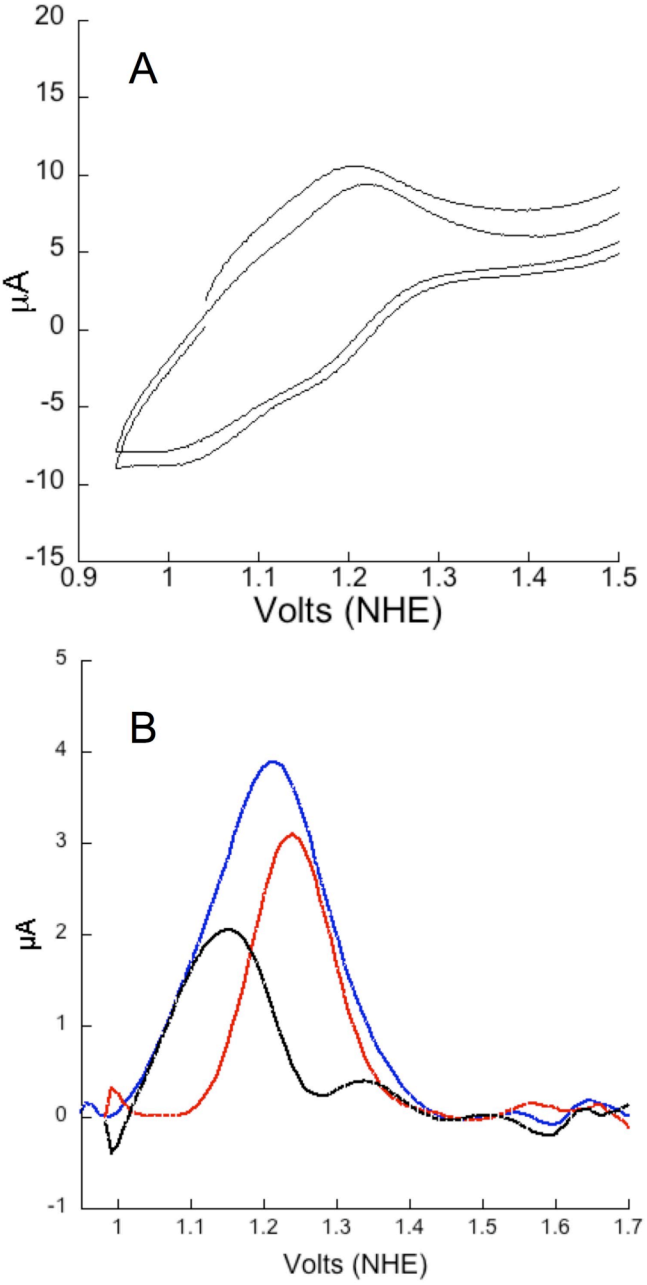

Figure S3 A) CV showing the unbuffered redox chemistry of **1** at pH = 5.10. B) The oxidation portion of the CV, as shown in part A, after baseline adjustment and fitting with an ideal line shape. The peak shape shown in black is assigned to complex **1** while a Mn(II) impurity is shown in red. The CV was taken at a basal plane graphite electrode in H_2O + 0.1 M KNO_3 scanned at 40 mV/s.

S3.0 Measuring the P_c^1 potential in unbuffered solution

Normally electrochemical potentials are reported as $E_{1/2}$ potentials but in this paper we have reported all of our data as the potential for the oxidation of **1** and avoided the midpoint potential entirely. The reason for this departure from normal procedure can be found by following the potential of P_c^1. As shown in figure S4 when we graphed the potential of P_c^1 vs. P_a^1 we found that the two lines intersected even though they should always remain parallel. This behavior was doubly confusing because P_c^1 and P_a^1 behave in a perfectly normal manner when buffer is present as shown in figure S5. As shown in figure S4 we eventually determined that this behaviour was linked to how far above the potential of Pa1 we scanned to. This discovery leads us to the conclusion that the Mn(II)(H_2O) present in unbuffered solution has a reduction peak hidden beneath the P_c^1 and P_c^2 peaks. Due to the difficulty in deconvoluting three overlapping peaks we decided to report our data as the anodic potential rather than the midpoint potential.

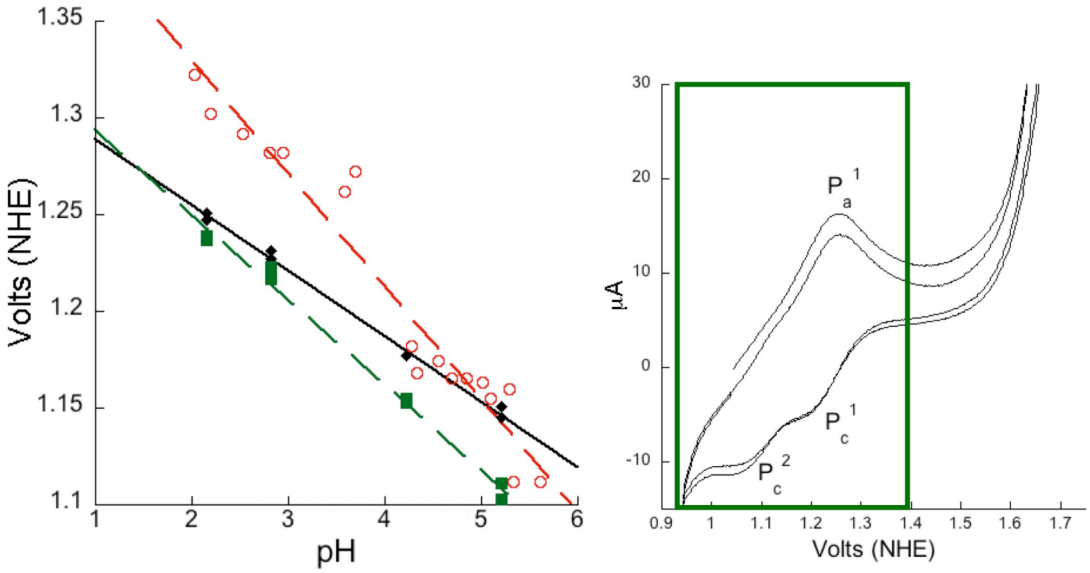

Figure S4 Right: CV of **1** in unbuffered aqueous solution scanned to 1.7 volts vs. NHE; the green box shows the area scanned when the upper potential limit is set to 1.4 volts vs. NHE. Right: A potential vs. pH plot showing the unbuffered oxidation potential P_a^1 (red circles), the unbuffered reduction peak P_c^1 when scanned to 1.7 volts (black diamonds) and when scanned to only 1.4 volts (green squares). All CVs taken at a basal plane graphite electrode in H_2O + 0.1 M KNO_3 and 1.0 mM **1** scanned at 40 mV/s.

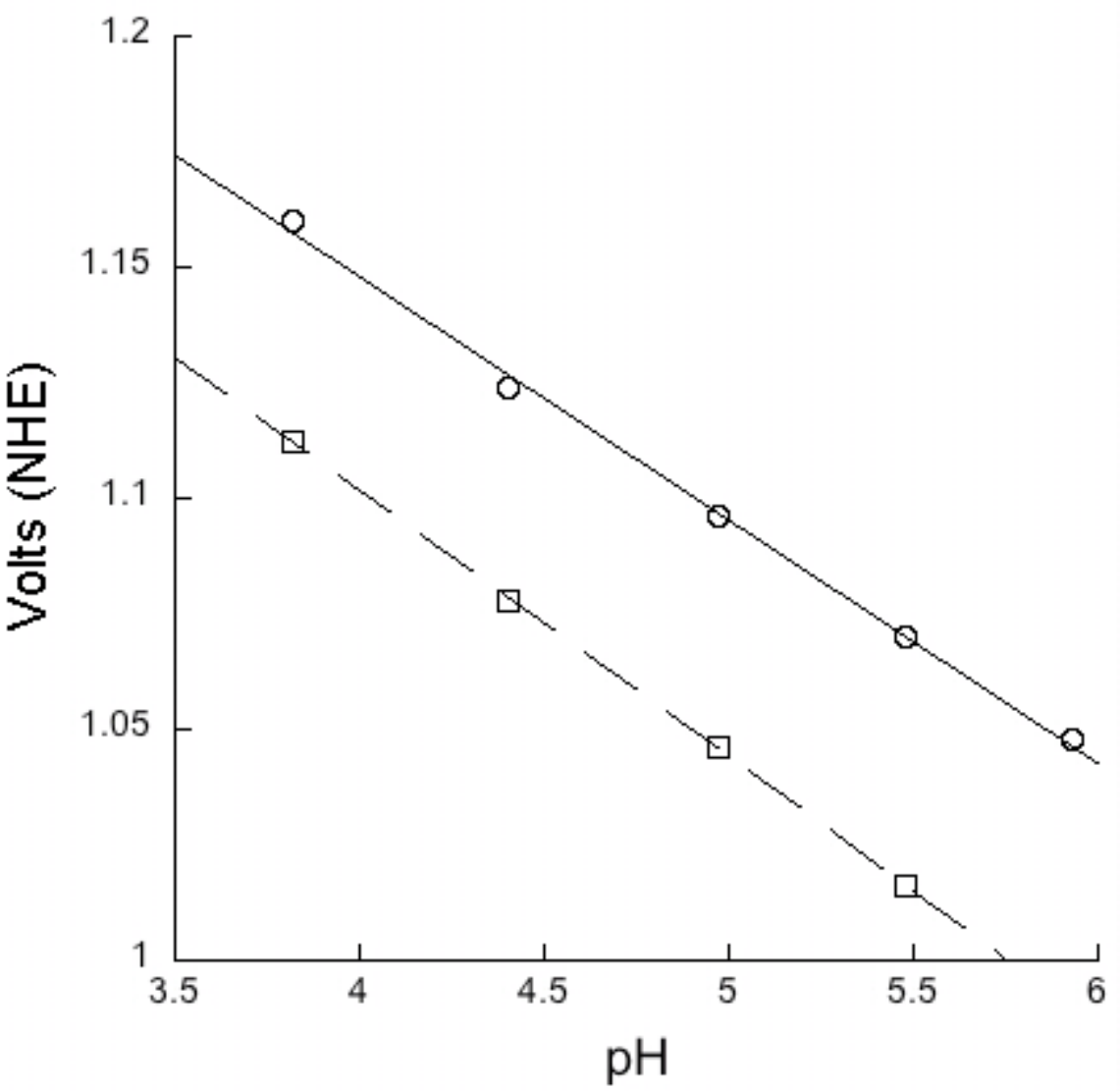

Figure S5 A plot of the pH dependence of oxidation P_a^1 (circles) and reduction P_c^1 (squares) of 2 mM **1** in 250 mM OAc buffer. The oxidation of **1** is fit to a straight line with a slope of 58 mV/pH while the reduction is fit to a slope of 56 mV/pH. All CVs taken at a basal plane graphite electrode in H_2O + 0.1 M KNO_3 scanned at 40 mV/s.

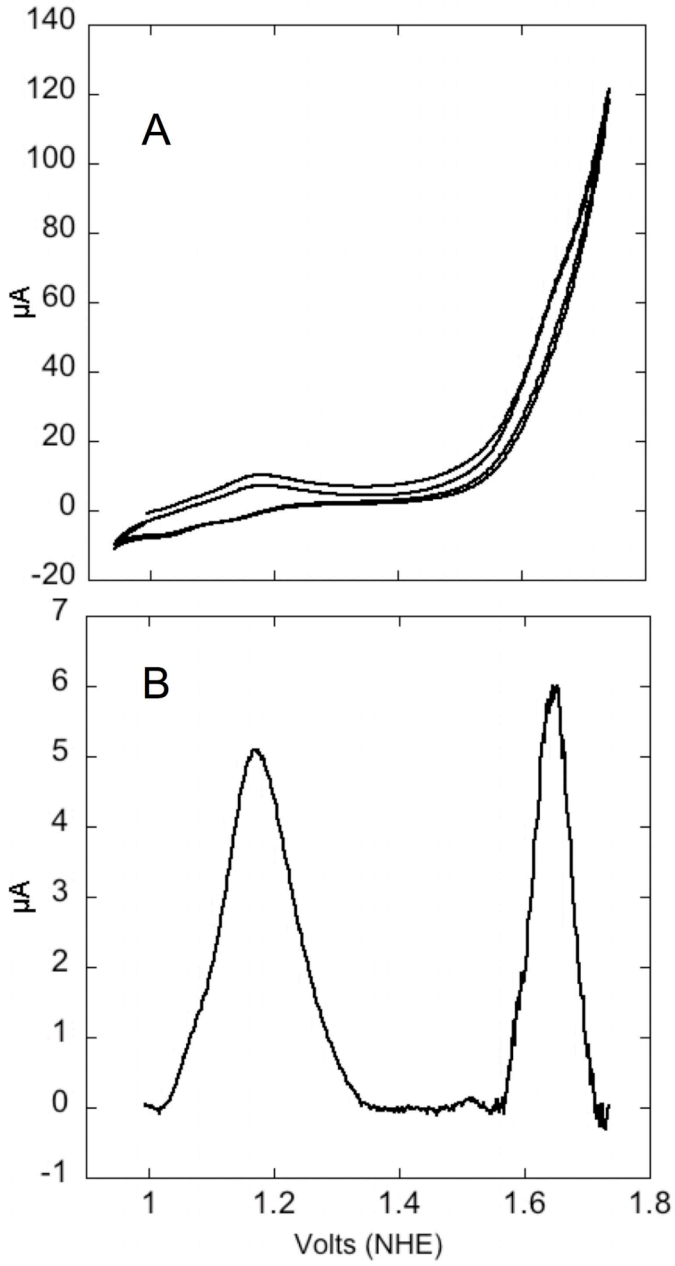

Figure S6. A) CV of 2 mM **1** in 150 mM acetate buffer at pH = 3.75. A second oxidation peak is observed at approximately 1.6 volts. CV taken at a basal plane graphite electrode in H_2O + 0.1 M KNO_3 scanned at 40 mV/s. B) Baseline corrected CV using a cubic splines method explained in greater detail above in the supplementary material.